Faculty Publications from the Department of Electrical and Computer Engineering

Electrical & Computer Engineering, Department of

2009

Ground-plane quasicloaking for free space

Efthymios Kallos
University of London - Queen Mary and Westfield College, themos.kallos@elec.qmul.ac.uk

Christos Argyropoulos
University of London - Queen Mary and Westfield College, christos.argyropoulos@unl.edu

Yang Hao
University of London - Queen Mary and Westfield College, yang.hao@elec.qmul.ac.uk

Ground-plane quasicloaking for free space

Efthymios Kallos,[*] Christos Argyropoulos, and Yang Hao[†]

School of Electronic Engineering and Computer Science, Queen Mary University of London, Mile End Road,
London E1 4NS, United Kingdom

Ground-plane cloak designs are presented, which minimize scattering of electromagnetic radiation from metallic objects in the visible spectrum. It is showed that simplified ground-plane cloaks made from only a few blocks of all-dielectric isotropic materials, either embedded in a background medium or in free space, can provide considerable cloaking performance while maintaining their broadband nature. A design which operates isolated in free space that cloaks radiation originating from a specified direction is also analyzed. These schemes should be much easier to be demonstrated experimentally compared to full designs.

PACS number(s): 42.79.−e, 02.40.−k, 41.20.−q

Transformation electromagnetics allows the manipulation of light in unprecedented ways such as the design of invisibility cloaks [1]. Most notably, a dispersive approximate cylindrical cloak that can be placed in free space was constructed using metamaterial-based resonating structures and was demonstrated to work in the microwave regime [2]. However, due to causality constraints [3,4], the required material anisotropy of such designs can only be achieved through increased absorption [5] and through sacrificing the bandwidth of operation [6]. In order to find a way around these issues, a different transformation that produces a design which transforms an object to a metal sheet was proposed [7]. In this scenario, the object is only cloaked when placed above a ground plane and the whole device needs to be embedded in a background material. However, it has the advantages that the material anisotropy can be so minimal that the cloak works well if the anisotropy is simply ignored. This approach was verified experimentally first by constructing a broadband microwave cloak using metamaterial elements operating nonresonantly [8], and later near 1.5 μm wavelengths using nanometer-size elements [9]. Still, the cloaks demonstrated require a background medium and were built using thousands of metamaterial cells, which is a challenge for an optical cloaking design due to the required subnanometer tolerances [10].

In this paper finite-difference time-domain (FDTD) simulations [11] are performed to test simplified broadband ground-plane cloak designs that operate in the optical frequencies, embedded either in a background material or in free space. These designs are considered as quasicloaks, in the sense that they are not aimed at providing perfect cloaking, but rather use the main physical principles of transformation electromagnetics in order to minimize the scattering signatures of metallic objects. First, it is showed that a simplified quasicloak consisting of only six unique blocks of conventional materials (with relative permittivities $\varepsilon > 1$) can provide very good ground-plane cloaking, after ignoring the anisotropy introduced from the initial transformation. Second, by further ignoring dispersive permittivity values

($\varepsilon < 1$), it is showed that a similar simplified ground-plane quasicloak designed to be embedded in free space minimizes scattering, without requiring a surrounding impedance-matched layer. The performance of the quasicloaks is confirmed by evaluating the spatial and spectral distributions of the scattered field energy. Finally, a simplified optical quasicloak is analyzed that operates directionally in air but without requiring a ground surface, a design that works similar to the optical mirage effect. These cloaks are isotropic, broadband, in principle lossless, and can be constructed with only a few all-dielectric blocks of conventional materials, which should pave the way to demonstrate them experimentally at optical frequencies.

A two-dimensional (2D) geometry is considered, where a metallic object is placed on a flat metallic ground plane. The object to be cloaked has a triangular shape with a height of 0.25 μm and base of 1.8 μm, and it is initially embedded in a glass material with $\varepsilon_{ref}=2.25$. The cloak is placed around the object covering a region 3 μm wide and 0.75 μm tall. The permittivity distribution inside the cloak is found by generating a map that consists of 64×15 nonorthogonal cells, which compresses the space occupied by the object inside the cloaked region [7], as shown in Fig. 1(a). Given the 2×2 covariant metric g for each cell [12,13], the relative permittivity of each block is found as $\varepsilon = \frac{\varepsilon_{ref}}{\sqrt{\det g}}$ [8,14]. A suitable map that reduces the anisotropy of the cloak is found by minimizing the width of the distribution of the parameter $\sqrt{\frac{g_{xy}g_{yx}}{g_{xx}g_{yy}}}$. For the map shown in Fig. 1(a), $1.79 \leq \varepsilon \leq 4.70$ and the maximum anisotropy is 1.20. The latter value can be reduced more by choosing to cloak an object with less sharp corners, however, it is preferred here because the cloak can be constructed in a simple manner using straight cuts.

Next, an orthogonal grid generated by recursive division of Cartesian cells is used to sample the original permittivity distribution of Fig. 1(a), as shown in Fig. 1(b). The sampled map consists of 80×20 square blocks that have dimension equal to 0.0375 μm. In addition, a low-resolution sampled map (quasicloak) is generated, consisting of 6×2 blocks that have dimensions 0.4285 μm by 0.3750 μm, as shown in Fig. 1(c). Some of the blocks are truncated to fit around the object. The latter quasicloak has $2.18 \leq \varepsilon \leq 3.30$. From the point of view of an impinging electromagnetic wave, these two cloaks should behave similarly if its wavelength is not

─────────
*themos.kallos@elec.qmul.ac.uk
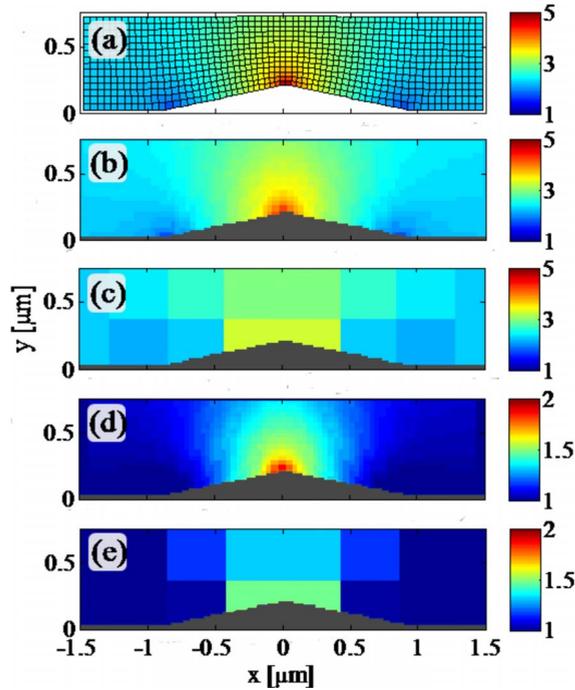†yang.hao@elec.qmul.ac.uk

FIG. 1. (Color online) Relative 2D permittivity maps for cloaking a triangular metallic object placed over a ground plane. The cloaks in (a)–(c) are embedded in glass (ε_{ref}=2.25), while the cloaks in (d) and (e) are embedded in free space (ε_{ref}=1). The colored bars indicate the relative permittivity values for each map. (a) Full nonorthogonal map consisting of 64×15 cells. (b) High-resolution sampled map consisting of 80×20 blocks. (c) Low-resolution sampled map consisting of 6×2 blocks. (d) High-resolution sampled map consisting of 80×20 blocks. (e) Low-resolution sampled map consisting of 4×2 blocks.

much smaller than the sizes of the blocks that consist the cloaks. In order to verify this claim, the performance of both cloaks is measured by using FDTD simulations with a resolution of 0.017 μm, assuming a 2.4 μm wide [full width at half maximum (FWHM)], 400 THz (in free space) TM Gaussian beam is incident at a 45° angle onto the object (from the $x < 0$ region). For this beam the free space wavelength is λ_0=0.750 μm. The simulation results are shown in Figs. 2(a)–2(c), when the anisotropy is ignored through setting the relative permeability of the device to μ=1.

The scattering off the aforementioned triangular metal object is shown in Fig. 2(a), where two distinct energy side lobes are observed. When the high-resolution cloak of Fig. 1(b) is placed around the object though, the reflection pattern of the scattering off a flat metallic plane is mostly restored and a single beam is observed again near 45°, as shown in Fig. 2(b). Any imperfections from the ideal reflected pattern are attributed to the ignored anisotropy and can be mediated by using a larger cloaked region and/or a smoother object. Next, when the low-resolution quasicloak of Fig. 1(c) is placed around the object, we observe in Fig. 2(c) that the cloaking performance is almost identical to the performance of the high-resolution cloak [Fig. 2(b)], thus verifying that ground-plane quasicloaking can be achieved with a very simple structure.

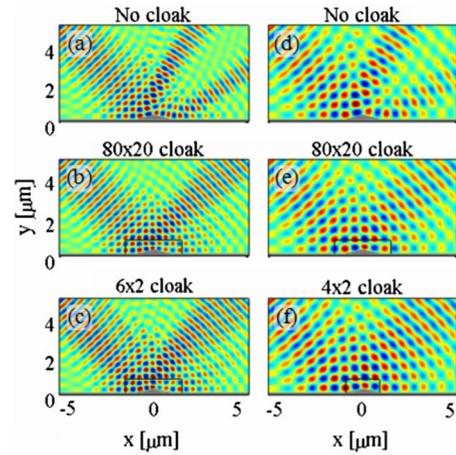Subsequently, the performance of a ground-plane cloak

FIG. 2. (Color online) Electric-field amplitude distribution for a 2.4-μm-wide, 400 THz Gaussian pulse impinging at 45° angle with respect to the normal to a conductive plane. The locations of the cloak and the object are outlined. [(a)–(c)] The background material is glass. [(d)–(f)] The background material is free space. [(a) and (d)] Scattering from a triangular metallic object. [(b) and (e)] Cloaks comprising of 80×20 blocks cover the object. [(c) and (f)] Simplified cloaks comprising of (d) 6×2 and (h) 4×2 blocks, respectively, cover the object.

embedded in free space is evaluated. A map similar to the one presented in Fig. 1(a) is generated, with the difference that it is surrounded by free space with ε_{ref}=1. Unavoidably, the transformation generates cells near the base corners of the triangular object that correspond to permittivity values that are smaller than the background permittivity ε_{ref}, with a minimum value equal to ε=0.8. As it will be shown in detail later, since these regions are relatively small compared to the total size of the cloak and compared to the incident wavelength, they are not expected to impact the cloaking performance significantly. Thus, a sampled high-resolution cloak is generated for free space, consisting of 80×20 blocks, and any smaller than unity values of the permittivity are set to 1, as shown in Fig. 1(d). In addition, a low-resolution quasicloak is obtained by sampling the latter high-resolution permittivity map. This quasicloak is shown in Fig. 1(e) and consists of 4×2 blocks with the following relative permittivity values in the $x < 0$ domain (left to right, top to bottom): [1.17, 1.30, 1.02, 1.47] [15]. The quasicloak is symmetric around x=0. The simulation results, when the previously described Gaussian beam impinges on this quasicloak, are shown in Figs. 2(d)–2(f), where it is observed that the field pattern of the cloaked object is very similar when either the low-resolution map [Fig. 2(f)] or the high-resolution map [Fig. 2(e)] is used. Again, the reflected beam pattern of the flat surface in free space is mostly restored from the two-lobe scattering pattern of the bare object [Fig. 2(d)].

The performance of nondispersive cloaks under broadband illumination has been studied analytically in [16,17]. Here, in order to quantify the performance and also verify the broadband cloaking capabilities of the ground-plane free space quasicloak of Fig. 1(e), a 2.4-μm-wide, 4.7-fs-long, TM Gaussian pulse around 600 THz is launched at 45° (in the $x < 0$ region) against the quasicloaked object. The total
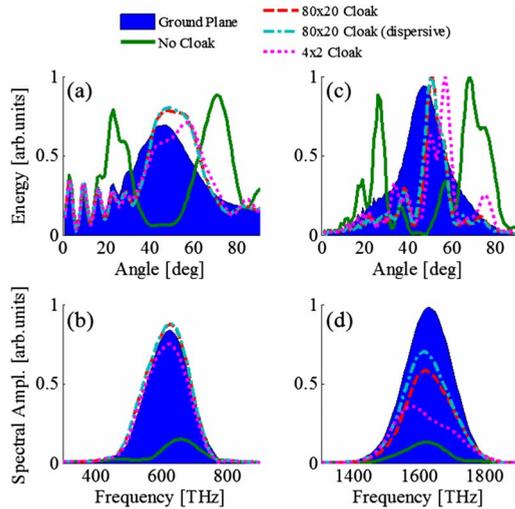
FIG. 3. (Color online) (a) Angular distribution of the scattered field energy in free space when a 4.7-fs-long, 2.4-μm-wide, 600 THz Gaussian pulse is incident. The patterns shown correspond to incidence on a flat plane, incidence on the metallic object placed on the plane, and incidence on the same object when covered with either the 80×20 [Fig. 1(d)], the 80×20 dispersive, and the 4×2 [Fig. 1(e)] quasicloaks. (b) The corresponding amplitudes of the frequency spectra of the scattered 600 THz pulse as recorded at a 45° angle. [(c) and (d)] The angular (c) and frequency (d) spectra of a 1600 THz scattered pulse in the same setup.

field energy crossing a semicircular curve with 4 μm radius centered at the object is recorded (in the $x > 0$ region). The pulse duration is chosen such that the frequency content of the pulse spreads over the whole visible spectrum: its FWHM is ≈ 250 THz.

The angular distribution of the reflected energy in the $x > 0$ region is shown in Fig. 3(a); the angles are measured from the ground plane. When only the flat ground surface is present, the peak of the distribution is observed at a 45° angle, as expected. When the metallic object is placed on top, however, two strong lobes are observed instead, at 23° and 71°. When the quasicloak based on the 80×20 map [Fig. 1(d)] is placed around the object, most of the scattered energy is now restored into a single lobe again around 49°. A similar single-lobe pattern is observed when the simplified sampled 4×2 quasicloak [Fig. 1(e)] is utilized, as shown also in Fig. 3(a), with only slight deterioration compared to the high-resolution cloak. The cloaking performance of simpler structures, consisting of fewer than eight blocks using this transformation map, is very limited. Note that the pattern observed for small angles (up to $\approx 20°$) in Fig. 3(a) is a result of the interference between the incident and reflected parts of the pulse.

In addition, the effect of the dispersive values of the original map that were ignored is analyzed. A dispersive FDTD simulation with similar parameters is performed, where the dispersive material parameters are mapped using the Drude model [18,19]. This simulation now includes the permittivity values $0.8 \leq \varepsilon < 1$ in the high-resolution 80×20 cloak, instead of setting that region to free space. The result of the angular distribution of the scattered energy for the dispersive

cloak is also shown in Fig. 3(a). Indeed, it is verified that the pattern is almost identical to the pattern of the nondispersive 80×20 cloak at that frequency.

The frequency spectra of the 600 THz scattered pulses are shown in Fig. 3(b), by recording the electric field amplitude as a function of time on the semicircular curve at a 45° angle. The filled area indicates the spectrum of the reflected pulse when only the flat surface is present, which is used as a reference. We observe in Fig. 3(b) that the frequency spectrum of the scattered pulse, when only the bare object is present on top of the ground plane, is severely distorted: both its amplitude is different compared to the reference spectrum, as well as its relative distribution within the spectrum. When the quasicloaks are covering the object, though, the spectrum of the original pulse at 45° is almost fully recovered. Again, the dispersive sections of the cloak do not affect its performance when replaced by free space.

The strong broadband performance of the quasicloak is exhibited until the incident wavelength becomes much smaller than the dimensions of the cloak's block elements. This is illustrated by launching an identical 4.7 fs long pulse at 1600 THz frequency toward the cloak and obtaining the reflected angular and spectral distributions as before, which are shown in Figs. 3(c) and 3(d), respectively. It is observed that the simplified 4×2 quasi-cloak is not capable of restoring either the scattering pattern or the spectrum as well as the 80×20 cloak. First, in Fig. 3(c), the angular distribution of the reflected energy when the cloaks are used deviates significantly from the ground-plane case, especially with the 4×2 cloak. Second, in Fig. 3(d), the reflected spectrum of the 1600 THz pulse is never fully restored, especially past 1550 THz. In addition, the dispersive cloak (with its elements tuned to operate around the incident frequency) now exhibits improved performance compared to the all-dielectric one. The dispersive area is larger in terms of the incident wavelength for this higher frequency, thus introducing more error when replacing it with free space.

The results of Fig. 3 demonstrate that even though perfect optical cloaking is not achieved with a quasicloak, its cloaking performance is substantial, with the additional advantages that it is very simple to construct and it can be natively placed in free space. These two factors are obviously extremely favorable in a variety of cloaking applications, as experimental imperfections that are inevitably introduced when building more complicated structures can be avoided. When designing a quasicloak, there is a tradeoff between the simplicity of the structure and the upper frequency of operation. While the broadband performance demonstrated here should be more than adequate for most applications, it can be improved when necessary by increasing the complexity of the structure.

The ground-plane quasicloaks discussed in this paper, so far, only work in the presence of a flat conducting surface. Next, we discuss a quasicloak design that can be placed isolated in free space, albeit working for a specified direction, as suggested in [7]. Starting with the quasicloak design of Fig. 1(e), the ground plane is removed and the cloaked region along with the object is mirrored around $y = 0$. As a result, a metallic diamond-shaped object is surrounded with a quasicloaking material consisting of 4×4 blocks. An incident
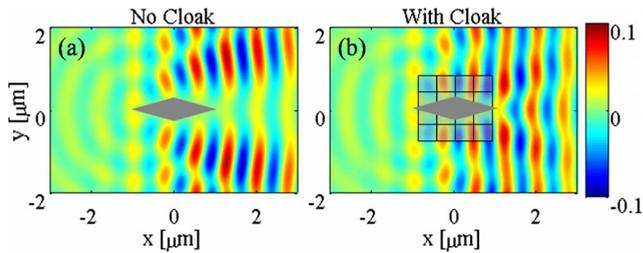
FIG. 4. (Color online) Electric-field amplitude distribution when a 12-fs-long, 400 THz Gaussian pulse impinges on a diamond-shaped metallic object in free space, parallel to its long axis. (a) Bare object. (b) Object covered with the proposed 4×4 simplified all-dielectric quasicloak.

electromagnetic wave would perceive a perfectly cloaked object as a collapsed strip of metal in the $y=0$ plane with—in principle—zero thickness. Suspended in free space, this device will scatter the impinging wave strongly for most incident angles, except when the wave is propagating parallel to the collapsed surface, i.e., along the x direction in this setup, for which the object would be effectively cloaked.

In Fig. 4(a) the electric-field amplitude distribution when a 12-fs-long, 400 THz TM Gaussian pulse is incident along the $+x$ direction on the bare object is shown, as calculated from FDTD simulations with the same discretization as before. A snapshot when the pulse has reached the $x>0$ region is depicted here. A very strong shadow is observed behind the object, along with a weak cylindrical scattering pattern in the $x<0$ region due to the sharp edge of the object at $x=-0.9$ μm. Subsequently, the aforementioned 4×4 quasicloak is placed around the object. We observe in Fig. 4(b) that now there is no shadow left as the wave fronts are bending and recomposing on the back of the object, with only slight distortion. Along the line of propagation ($y=0$ axis), the total field energy restored behind the object is improved approximately ten times compared to the noncloaked object. Despite the weak reflections that remain in the $x<0$ region, this indicates strong cloaking performance which is on par with the performance of the approximate cylindrical dispersive cloak [2,20]. The bandwidth tolerance is similar to the ground-plane cloak design of Fig. 3 (not shown), since the same design is utilized here. This scheme can be practical for a variety of cloaking applications, where the position of the observer is known in advance, e.g., for shielding objects placed in the line of sight of antennas or satellites. The scheme becomes increasingly favorable for quasicloaking objects in free space when considering its design simplicity, since only a few blocks of all-dielectric materials are required in order to achieve broadband lossless performance across the visible spectrum.

A physical explanation for the behavior of light waves in a ground-plane cloak, when the incidence occurs parallel to the ground plane [Fig. 4(b)], is obtained when considering the well-known optical mirage effect [21]. In the latter case, the path of incoming light rays is bent toward increasing refractive index gradients, typically caused by air density differences in the atmosphere. In a similar manner, light traversing a ground-plane cloak is bent toward higher refractive indices, originating from the electromagnetic transformation. Three distinct stages are observed. First, as the wave reaches the first corner of the object (at $x=-0.9$ μm), the index gradient is increasing away from the surface [see also the map on Fig. 1(a)], and thus the waves bend away from the object. Second, near the tip of the object (at the $x=0$ plane) the index gradient is reversed, causing the waves to bend back toward the object. Finally, due to the increasing index gradient away from the object near the second corner (at $x=+0.9$ μm), the waves are bent away from the object, and the original propagation parallel to the object's long axis is restored.

In conclusion, using FDTD simulations, it is demonstrated that ground-plane quasicloaks can be designed using relatively simple structures without significantly affecting their cloaking performance or bandwidth. Such a quasicloak designed to work in free space above a metallic surface, consisting of only eight all-dielectric blocks, can provide strong cloaking potential over the whole visible spectrum, as long as its features remain smaller than the wavelength of radiation. In addition, the quasicloak can operate without any flat surface present in free space for a specific angle of wave incidence, in analogy with the mirage effect. These designs should be straightforward to be practically implemented compared to previous ideas, e.g., by doping material blocks or by using nonresonant metamaterial cells.

[1] J. B. Pendry, D. Schurig, and D. R. Smith, Science **312**, 1780 (2006).

[2] D. Schurig *et al.*, Science **314**, 977 (2006).

[3] S. A. Tretyakov and S. I. Maslovski, Antennas and Propagation Magazine, IEEE **49**, 37 (2007).

[4] P. Yao, Z. Liang, and X. Jiang, Appl. Phys. Lett. **92**, 031111 (2008).

[5] S. Linden *et al.*, Science **306**, 1351 (2004).

[6] Z. Ruan *et al.*, Phys. Rev. Lett. **99**, 113903 (2007).

[7] J. Li and J. B. Pendry, Phys. Rev. Lett. **101**, 203901 (2008).

[8] R. Liu *et al.*, Science **323**, 366 (2009).

[9] Two preprints of papers that describe experimental results for all-dielectric cloaks in the optical regime have appeared after this paper was originally submitted: e-print arXiv:0904.3508; e-print arXiv:0904.3602.

[10] W. Cai *et al.*, Nat. Photonics **1**, 224 (2007).

[11] A. Taflove and S. C. Hagness, *Computational Electrodynamics: The Finite-Difference Time-Domain Method*, 3rd ed. (Artech House, Boston, 2005).

[12] J. F. Thomson, B. K. Soni, and N. P. Weatherill, *Handbook of Grid Generation* (CRC Press, Boca Raton, 1999).

[13] R. Holland, IEEE Transactions on Nuclear Science **30**, 4589

(1983).

[14] D. Schurig, J. B. Pendry, and D. R. Smith, Opt. Express **14**, 9794 (2006).

[15] Due to the coarse structure of this simplified cloak, the permittivity values obtained are always larger than unity, even if the dispersive version of the 80×20 map is sampled.

[16] R. Weder, J. Phys. A: Math. Theor. **41**, 065207 (2008).

[17] R. Weder, J. Phys. A: Math. Theor. **41**, 415401 (2008).

[18] Y. Zhao, C. Argyropoulos, and Y. Hao, Opt. Express **16**, 6717 (2008).

[19] C. Argyropoulos, Y. Zhao, and Y. Hao, IEEE Trans. Antennas Propag. **57**, 1432 (2009).

[20] S. Cummer *et al.*, Phys. Rev. E **74**, 036621 (2006).

[21] W. J. Humphreys, *Physics of the Air*, 3rd ed. (McGraw-Hill, New York, 1940).